PROCEEDINGS OF SPIE

SPIEDigitalLibrary.org/conference-proceedings-of-spie

Probing the backscattering of TiO2 particles with vortex beams

Zambrana-Puyalto, Xavier, Vidal, Xavier, Molina-Terriza, Gabriel

Xavier Zambrana-Puyalto, Xavier Vidal, Gabriel Molina-Terriza, "Probing the backscattering of TiO2 particles with vortex beams," Proc. SPIE 11345, Nanophotonics VIII, 1134507 (1 April 2020); doi: 10.1117/12.2555460

SPIE.

Event: SPIE Photonics Europe, 2020, Online Only

Probing the backscattering of TiO_2 particles with vortex beams

Xavier Zambrana-Puyalto[a,b], Xavier Vidal[a,c], and Gabriel Molina-Terriza[a,d,e]

[a]Department of Physics and Astronomy, Macquarie University, 2109 NSW, Australia;
[b]Istituto Italiano di Tecnologia, Via Morego 30, 16136 Genova, Italy;
[c]Fraunhofer Institut für Angewandte Festkörperphysik (IAF), Tullastrasse 72, 79108 Freiburg, Germany;
[d]Centro de Física de Materiales (MPC), Donostia International Physics Center (DIPC), 20018 Donostia-San Sebastián, Spain;
[e]IKERBASQUE, Basque Foundation for Science, 48013 Bilbao, Spain

ABSTRACT

We present a set of experiments in which the backscattering spectra of 4 μm single TiO_2 particles are probed with circularly polarized vortex beams. The experiment is carried out with a tunable laser at $\lambda = 760 - 810$nm. We observe that the use of vortex beams enables us to tailor the backscattering in different ways. Given a certain backscattering of a particle (induced by a Gaussian beam or a plane wave), we observe that vortex beams can tune it and sharpen it. Moreover, we also observe that the level of conservation of helicty can be increased thanks to the use of vortex beams. We explain the mechanisms that give rise to these effects using Mie Theory. Our method of backscattering control can be experimentally implemented in most of microscopy set-ups. In addition, if brought to its limits, the method can be used to excite single multipolar modes from spheres. We believe that our method could find application in the levitation of particles or the excitation of whispering gallery modes.

Keywords: Mie Theory, multipoles, vortex beams, helicity, angular momentum, phase singularity, whispering gallery modes

1. INTRODUCTION

Light scattering from particles is an old problem in optics. Different descriptions can be used: ray optics, wave optics or electromagnetic (EM) optics. In EM optics, in order to get an accurate result, Maxwell equations need to be solved. This implies that for most problems, the solutions are not analytical and different approximations are necessary. However, the scattering of a plane wave with a homogeneous sphere was found to have an analytic solution by Lorenz and Mie in 1898 and 1908 respectively.[1,2] Since then, Mie theory has been used to describe an innumerable amount of scattering phenomena. In fact, the reach of Mie theory took a big step forward in the 1990s when the theory was extended to any kind of incident beam of light.[3] Thanks to these advances, the interaction between lasers and particles could be described in a more accurate manner. Also in the 1990s, the field of the angular momentum (AM) of light took a big leap forward. With the seminal paper of Allen and co-workers,[4] it became clear that the AM of light could be controlled using available elements such as quarter-wave plates and computed generated holograms. In the beginning, the AM was specially used in optical tweezers and in quantum information.[5–9] Yet, approximately since 2007, the AM also started to be used to probe the scattering of spheres[10–18] and other nanostructures.[19–24] As a result, new discoveries have been made in diverse fields such as sensing,[25–28] chirality,[29–32] or even quantum optics.[33–35]

In this work, we experimentally study the interaction between vortex beams and TiO_2 micron-sized single spheres deposited on top of a microscope slide. We observe that the AM of light of these vortex beams modifies the backscattering cross section (BCS) of the sphere. We observe that the AM content of the beams shifts and sharpens the peaks of the BCS, as predicted in Refs. 36,37. Finally, we observed that the minima and maxima of a BCS have very different spatial properties, and we will relate them to the helicity[38–40] content of the beam.

Nanophotonics VIII, edited by David L. Andrews, Angus J. Bain, Martti Kauranen, Jean-Michel Nunzi, Proc. of SPIE Vol. 11345, 1134507 · © 2020 SPIE
CCC code: 0277-786X/20/$21 · doi: 10.1117/12.2555460

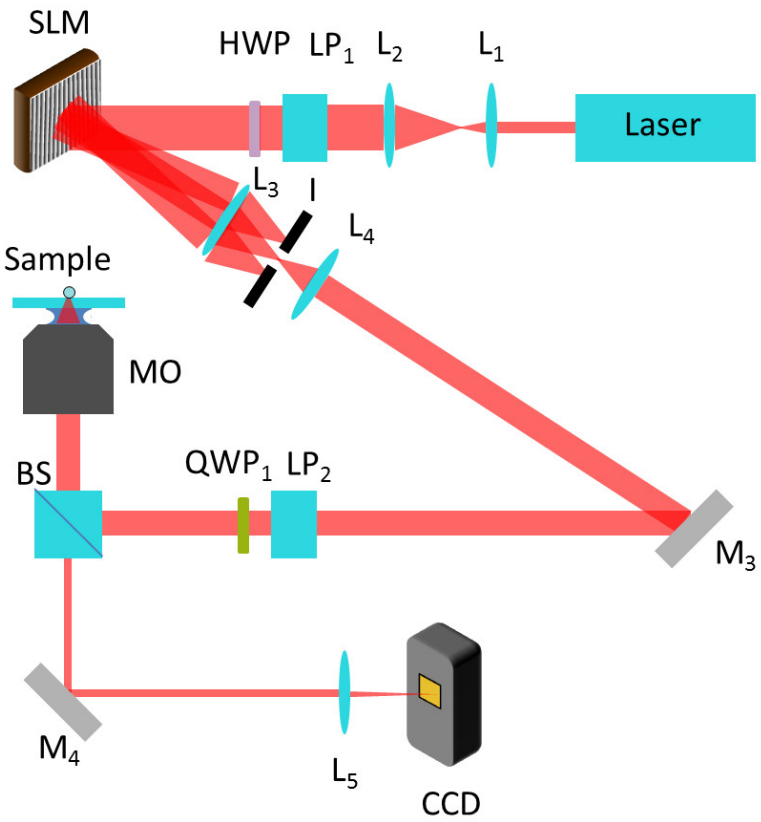

Figure 1: Schematics of the experimental set-up. A laser beam of variable wavelength $\lambda = [760 - 810]$nm is expanded with two lenses (L_1, L_2) and polarized with a linear polariser (LP_1) and a half-wave plate (HWP) to match the requirements of the spatial light modulator (SLM). The SLM gives the desired spiral phase to the beam, and the first diffraction order is selected with the combined use of two lenses (L_3, L_4) and an iris (I). The two lenses are simultaneously used to expand the beam and match its size to the back-aperture of the microscope objective (MO). Later, the polarisation of the beam is modified with a linear polariser (LP_2) and a quarter-wave plate (QWP_1). Then, the beam is focused down to the sample using a MO and the backscattering is collected using a beam splitter (BS). The backscattered light is imaged onto a CCD camera using L_5

2. EXPERIMENTAL DETAILS

The experimental set-up is schematically displayed in Figure 1. A tunable fibred laser diode yielding a Gaussian mode is linearly polarized and then it illuminates the chip of a spatial light modulator (SLM). Afterwards, the SLM modifies the phase of the beam to create a vortex beam with a phase singularity of order l. Because the SLM position is static but its phase depends on λ, a small correction has to be given at every single wavelength so that the optical singularity is well-aligned with the propagation axis of the set-up. Then, the first diffraction order is selected using a pair of lenses and an iris (L_3, L_4 and I). The polarization of this first diffraction order is modified to create a state of well-defined helicity[24,32,41] with a linear polariser and a quarter-wave plate (LP_2 and QWP_1). Because the beams are paraxial, we consider that a left circularly polarized (LCP) beam has $p = 1$, and a right circularly polarized beam (RCP) has $p = -1$. In addition, it can be demonstrated that a collimated beam with helicity p and a phase singularity of order l along its axis of propagation has a total AM along the same axis $m_z = l + p$.[24,32,41] Note that in order to get a pure state of helicity at every single wavelength of use, the QWP_1 needs to change its position at every single λ. After the QWP_1, our vortex beams have a well-defined energy, projection of the AM along the direction of propagation, and helicity; and their respective eigenvalues are $2\pi/\lambda$, $m_z = l + p$, and p. Then, using a 100x water-immersion microscope objective (MO), the light beam is focused onto the sample. The MO has an NA= 1.1, and it is attached to a z-translation stage. Due to chromatic aberrations, we make sure that the plane of the sample is the focal plane for every wavelength. The sample is a set of single TiO_2 (amorphous crystal phase) particles deposited on top a microscope slide. The TiO_2 particles have been deposited via spin-coating yet the separation among them is not constant. In order to avoid any coupling effects, we have only probed particles which are more than 20μm apart. The titania particles have a radius $R = 2\mu m$, and their index of refraction in air is $n_r = 1.8$. The slide is placed on a sample holder which is attached to a nano-positioning device. We use these positioning devices to center the optical singularity of the incident vortex beam with the center of the particle. This process is done in real time by looking at the reflected intensity pattern with a CCD camera. The same CCD camera is used to measure the backscattering. The backscattering is collected with the same MO used to focus the light on the sample. Then, a beam-splitter (BS) is used to separate the backscattered light from the incident beam. Afterwards, the beam goes through a lens (L_5) that images the sample onto a CCD camera. In order to measure the backscattering, three different power measurements are carried out: P_0, P_p, P_s (see their definition below). The three of them are done using the same CCD camera and integrating the single pixel contributions. Great care has been taken not to saturate the CCD camera. In order to do that, each wavelength measurement is associated to an exposure time (E) and a filter value (F). Then, if a signal S_I is obtained after integrating the values of all the active pixels of the CCD, the real signal is obtained doing $S_{I'} = S_I/(E \cdot F)$. The previous formula assumes a linear response of the system, which is the case in our set-up due to the moderate power of the laser $< 50mW$. Now, P_p is the measurement of the backscattering of the particle. P_s is the measurement of the backscattering of the the substrate when the particle is displaced $10\mu m$ from it. And P_0 is the noise measured by the CCD camera when the laser is switched off but all the rest of devices are on. With these three measurements, we compute:

$$I = \frac{P_p - P_0}{P_s - P_0} \tag{1}$$

which is a dimensionless number that characterizes the backscattering of the particle that is being probed. In fact, it is a measurement of the backscattering signal normalized to the backscattering of the substrate and background corrected.

3. EXPERIMENTAL RESULTS

For this set of measurements, we have used vortex beams with phase singularities of the order $l = 0, \pm1, \pm2, \pm6, \pm7$. The wavelength of the monochromatic laser has been varied from 760 to 810nm in steps of $\Delta\lambda = 4$nm. In Figure 2 we show all our spectral measurements. In both Figure 2a and Figure 2b we plot wavelength scans of the backscattering of the TiO_2 particles from $\lambda = 760 - 810$nm. As mentioned above, the backscattering is given as a ratio of the signal with the particle over the signal without the particle, yielding a dimensionless number I. In order to make the plots clearer, we have divided the spectral measurements in two subfigures, Figure 2a for

Further author information: Send email to X.Z.-P.: E-mail: xavislow@protonmail.com

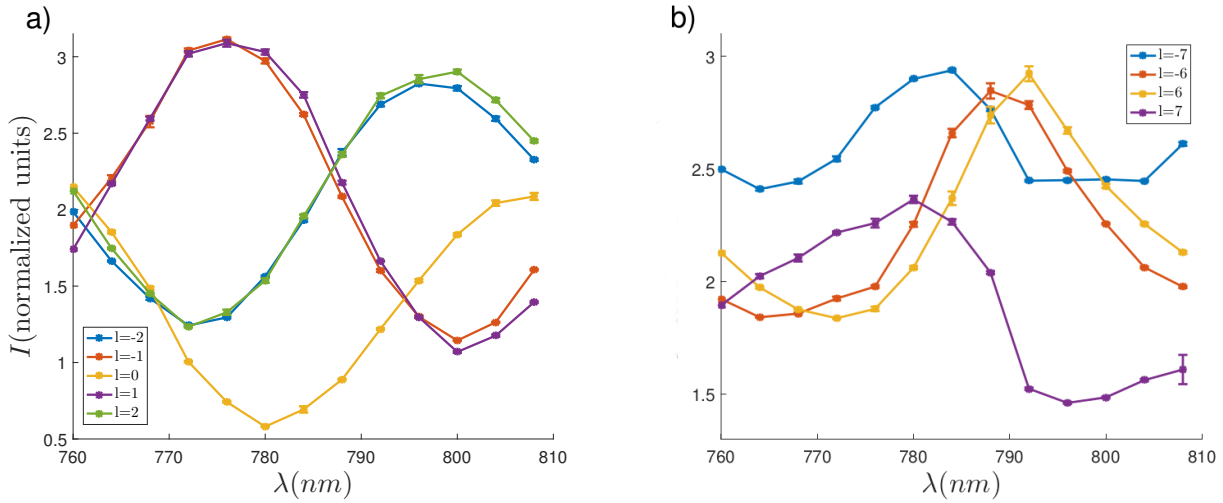

(a) $l = 0, \pm 1, \pm 2$ (b) $l = \pm 6, \pm 7$

Figure 2: Wavelength scan of backscattering spectra of 4 μm TiO_2 particles placed on top of a microscope slide. The wavelength scan is varied from 760 to 810nm in steps of $\Delta\lambda = 4$nm. The signal is normalized to the power of the corresponding reflected beam at the glass-air interface following Eq.(1).

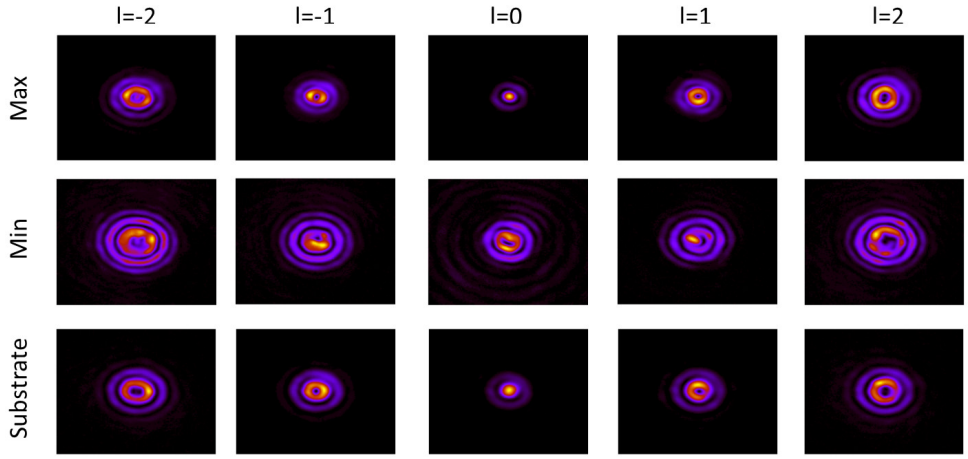

Figure 3: Snapshots of the backscattering of the 4 μm TiO_2 particles for incident beams with phase singularities of $l = 0, \pm 1, \pm 2$. The maxima and the minima are taken at their corresponding wavelength, *e.g.* at 782nm for $l = 0$'s minimum (see Figure 2a). The snapshot taken for the substrate backscattering is taken at the maxima's wavelength.

$l = 0, \pm 1, \pm 2$ and Figure 2b for $l = \pm 6, \pm 7$. The helicity of the beam is $p = 1$ for both cases. In Figure 2a the plots for vortex beams of $l = 0, \pm 1, \pm 2$ are depicted. All the plots have an oscillating behavior. It is observed that the Gaussian beam ($l = 0$) yields a minimum of backscattering at $\lambda = 782$nm. In contrast, the beams with $l = \pm 1, \pm 2$ have both a maximum and a minimum in the probed range. We see that the beams with the same $|l|$ yield the same backscattering result. In exchange, in Figure 2b, we see some different effects. Firstly, the beams with the same $|l|$ do not yield the same result - even though they still resemble each other. Furthermore, in comparison to Figure 2a, we observe that the oscillating behavior is shifted and sharpened.

As mentioned in section 2, all the experimental measurements are done with a CCD camera. Integrating

over the pixels of the camera, we can measure the dimensionless BCS given by I (see Eq.(1)). Yet the images captured with the CCD can also be used to obtain some spatial information about the backscattered field. For that matter, we plot them in Figure 3. Figure 3 has five columns, each of them showing the backscattering obtained with an incident beam with a given $p = 1$ and l. The two upper rows of Figure 3 show the signal at the CCD camera at different λ conditions, namely the maxima and minima obtained in Figure 2a. The third row shows the backscattering pattern of the substrate, *i.e.* we obtained them when the particle was moved away from the incident beam. The substrate images are taken at the maxima wavelength, but it has been verified that their backscattering pattern remains the same for the whole studied spectral range. Now, by comparing the two upper rows, it is observed that the spatial properties of the backscattered field vary significantly even in such a small wavelength range. Moreover, we observe that the images at the maxima and substrate rows are almost identical.

4. DISCUSSION

Let us discuss the results presented in the previous section. First of all, Figure 2 shows us that the backscattering presents an oscillating behavior in the studied wavelength range. Furthermore, it is seen that the oscillating behavior of the Gaussian beam can be shifted and narrowed thanks to the AM content of the beam. Here, it is important to differentiate between oscillating and resonant behavior. The optical resonances of a system happen at well-defined wavelengths, λ_r. Their values entirely depend on the material and geometry of the system, but never on the excitation.[42–44] Thus, none of the peaks observed in Figure 2 can be due to a resonance, as if that was the case, they would stay fixed at λ_r. Now, if they are not resonances, and therefore they are oscillations, one should still wonder what these oscillations are due to, and why they can be shifted and sharpened with the AM of light. Next, we will argue that the oscillations are a weighted superposition of many different modes of the sphere, and that their weight can be tailored by the excitation. In order to do that, some theoretical background needs to be introduced, namely Mie Theory. Due to the substrate where the particles are lying, the single particles of the experiment do not fulfil the assumptions of Mie theory. Still, Mie Theory proves to be a good theoretical framework to discuss the results. In Mie theory, the scattered field off a particle is analytically found once the illumination has been decomposed into multipolar modes $\left\{\mathbf{A}^{(e)}_{jm_z}, \mathbf{A}^{(m)}_{jm_z}\right\}$.[36,37,40,45] That is, if the incident beam is expressed as $\mathbf{E^i} = \sum_{j,m_z} \alpha^{(e)}_{j,m_z}\mathbf{A}^{(e)}_{jm_z} + \alpha^{(m)}_{j,m_z}\mathbf{A}^{(m)}_{jm_z}$, where $\alpha^{(e)}_{j,m_z}$ and $\alpha^{(m)}_{j,m_z}$ are general coefficients that modulate the multipolar decomposition, then the scattered field is:

$$\mathbf{E^s} = \sum_{j,m_z} \left[\alpha^{(e)}_{j,m_z} a_j \mathbf{A}^{(e)}_{jm_z} + \alpha^{(m)}_{j,m_z} b_j \mathbf{A}^{(m)}_{jm_z}\right] \tag{2}$$

where a_j, b_j are the so-called Mie coefficients. Due to the orthonormality relations between $\mathbf{A}^{(e)}_{jm_z}$ and $\mathbf{A}^{(m)}_{jm_z}$, the scattering cross section is computed as:

$$C_s \propto \sum_{j=1}^{\infty} \sum_{m_z=-j}^{j} \left(|\alpha^{(e)}_{j,m_z} a_j|^2 + |\alpha^{(m)}_{j,m_z} b_j|^2\right) \tag{3}$$

Now, as mentioned before, we can define the vortex beams used for this experiment as a function of λ, p, m_z. Hence, we will denote $\mathbf{E}^{\lambda}_{p,m_z}$ as the incident monochromatic beam with helicity p, and AM m_z. It can be proven that $\mathbf{E}^{\lambda}_{p,m_z}$ are cylindrically symmetric.[24] Now, in Refs. 36, 37, it was demonstrated that if $\mathbf{E^i} = \mathbf{E}^{\lambda}_{p,m_z}$, then

$$C_s \propto \sum_{j=|m_z|}^{\infty} |C_{jm_z}|^2 \left(|a_j|^2 + |b_j|^2\right) \tag{4}$$

where C_{jm_z} is the only set of coefficients that define the multipolar content of the incident beam. We will use Eq.(4) to discuss the experimental results. Indeed, notice that the coefficients C_{jm_z} (same applies to $\alpha^{(e)}_{j,m_z}, \alpha^{(m)}_{j,m_z}$) do not depend on the wavelength. Therefore, the wavelength dependence seen in Figure 2 needs to come from the Mie coefficients a_j, b_j. Moreover, when we modify the AM content of the beam (we change m_z) not only we modify

the function C_{jm_z} but also we change the amount of modes contributing to the superposition given by Eq.(4). That is, a given m_z of the incident beam ensures that the contribution of the lowest $j = (|m_z| - 1)$ multipoles is suppressed from the scattering.[16,36,37] Now, here we can distinguish between three scenarios depending on AM of the incident beam. If $m_z \gtrsim 2\pi n_r R/\lambda$, where n_r is the ratio between the index of refraction of the sphere and the medium surrounding it, the scattering of the particle is completely suppressed. Indeed, it can be checked that the Mie coefficients a_j and b_j are negligible for orders $j \gtrsim 2\pi n_r R/\lambda$.[16,40] If $m_z \sim 2\pi n_r R/\lambda$, a single multipolar mode can be excited.[16,36,37] This regime is particularly interesting for the excitation of whispering gallery modes[40,46,47] And if $m_z \lesssim 2\pi n_r R/\lambda$, which is the case of our experiment, different modes contribute to the scattering. That is, given a particle (R, n_r) and a wavelength λ, the lowest $j \approx 2\pi n_r R/\lambda$ multipolar modes will potentially contribute to the scattering. By increasing the AM content of the incident beam (m_z), the contribution of the first $j = (|m_z| - 1)$ is progressively suppressed, until there are no contributing modes. Now, because Mie resonances are narrow, it follows that the fewer number of contributing modes, the narrower the response of the system. This effect was theoretically shown in 36, 37, and we experimentally observe it in Figure 2 as well as in Ref. 18. Clearly, the oscillations depicted in Figure 2a are broader than those shown in Figure 2b.

The shift of the cross section is a subtle effect due to the superposition of different modes. Mie theory simulations show that the backscattering spectral response never resembles that of a single multipolar mode. Rather, the response of the particle is always a superposition of at least five multipolar modes. This feature highlights the fact that the spectral measurements shown in Figure 2 are oscillations of complex superpositions of Mie modes, and not resonant peaks. These complex superpositions give rise to local scattering minima and maxima, and these are the ones that we define as oscillations. When we change the incoming beam, we change the complex superposition of modes that give rise to oscillations, and hence, their spectral position can vary. In contrast, Mie resonances are always located in the same spectral position regardless of the incoming beam.

Finally, we set out to explain the root cause of the spatial differences put forward by Figure 3. The images displayed in Figure 3 are the backscattering recordings of the system (particle + substrate) under an incident illumination of the kind $\mathbf{E^i} = \mathbf{E}^{\lambda}_{p,m_z}$. Here, as in the rest of the paper, backscattering needs to be understood as the light scattered in the reflection semi-space (see Figure 1). Now, the scattering of a system can be divided into its two helicity component,[24,38,41,48,49] *i.e.* $\mathbf{E^s} = \mathbf{E^s_p} + \mathbf{E^s_{-p}}$, where the two components have a well-defined helicity.[24] Next, we are going to argue that the differences in the images stem from the relative difference between these two helicity components. But before, a point needs to be made about the substrate. As it was commented on the Results section, the substrate by itself yielded a very constant response as a function of the wavelength. It basically behaved as a mirror with a very low reflection. That is, the backscattered light off the substrate is a mirror image of the incident beam. Now, the mirror image of a beam $\mathbf{E}^{\lambda}_{p,m_z}$ is $\mathbf{E}^{\lambda}_{-p,m_z}$. Notice that a beam like $\mathbf{E}^{\lambda}_{-p,m_z}$ in the backward semi-space yields the same intensity pattern as $\mathbf{E}^{\lambda}_{p,m_z}$ in the forward semi-space.[40] That is why the third row of Figure 3 yields an approximate mirror image of the incident beam $\mathbf{E}^{\lambda}_{p,m_z}$. Now, in general we denote the scattered field off the system as $\mathbf{E^s}$. However, because the system is linear, and cylindrically symmetric, the system must preserve the wavelength λ and the AM of the incident beam, m_z. Hence, $\mathbf{E^s} \equiv \mathbf{E}^{\mathbf{s},\lambda}_{m_z}$. A mentioned before, the system does not preserve the helicity of light,[24,41] therefore the scattered field can be decomposed as $\mathbf{E}^{\mathbf{s},\lambda}_{p,m_z} + \mathbf{E}^{\mathbf{s},\lambda}_{-p,m_z}$. Now, as it is studied in Refs. 24, 41 these two helicity components have a very different spatial dependence. If we take as the incident beam a Gaussian beam $(l = 0)$ $\mathbf{E^i} = \mathbf{E}^{\lambda}_{p,m_z} = \mathbf{E}^{780}_{1,1}$, then the two backscattered helicity components are $\mathbf{E}^{\mathbf{s},780}_{-1,1}$, and $\mathbf{E}^{\mathbf{s},780}_{1,1}$. It can be seen that $\mathbf{E}^{\mathbf{s},780}_{-1,1}$ resembles the reflection of the substrate, whereas the other helicity component $\mathbf{E}^{\mathbf{s},780}_{1,1}$ resembles such of a vortex beam with $l = 2$.[24,41] And this is exactly what is observed at the minimum of the BCS - except for some experimental imperfections which lead the phase singularity of charge $l = +2$ split into two singularities of charge $l = +1$.[24,50] Thus, it seems as if the minima of the oscillations in the BCS were related to different relative importance of the two helicity components in the BCS. Mie theory simulations can be used to show that indeed the minima in the BCS correspond to approximately maxima in the $|\mathbf{E}^{\mathbf{s},\lambda}_{p,m_z}|/|\mathbf{E}^{\mathbf{s},\lambda}_{-p,m_z}|$ ratio.[18] That is, the minima of BCS are related to maxima in helicity preservation. Here, it is again observed that the AM plays a key role. Doing some extra Mie theory simulations for incoming beams with $m_z = 7, 8$, one can observe that it is no longer true that the minima of the BCS are related to approximate maxima of helicity preservation.[18] Furthermore, it is observed that as the AM gets increased, the helicity is more and more preserved - and effect

which was already predicted in Ref. 16.

5. CONCLUSION

In conclusion, we have experimentally shown that the AM of light plays a crucial role in the light scattering of spherical particles. We have observed that by increasing the AM of the illumination, not only the scattering response can be tuned and sharpened, but also the preservation of helicity by a sphere can be improved by orders of magnitude. To show that, the backscattering of TiO_2 particles deposited on a glass substrate has been experimentally measured. The findings of this paper are of relevant to potentially address single multipolar resonances for systems whose sizes are of the order of the wavelength or smaller.

ACKNOWLEDGMENTS

X.Z.-P. acknowledges funding from the European Union's Horizon 2020 research and innovation programme under the Marie Sklodowska-Curie grant agreement No 795838.

REFERENCES

1. L. Lorenz, "Sur la lumière réfléchie et réfractée par une sphère transparente," *Oeuvres scientifiques de L. Lorenz. revues et annotées par H. Valentiner. Tome Premier, Libraire Lehmann & Stage, Copenhague* , pp. 403–529, 1898.
2. G. Mie, "Beiträge zur optik trüber medien, speziell kolloidaler metallösungen," *Annalen der Physik* **330**(3), pp. 377–445, 1908.
3. G. Gouesbet and G. Gréhan, *Generalized Lorenz-Mie Theories*, Springer, 2011.
4. L. Allen, M. W. Beijersbergen, R. J. C. Spreeuw, and J. P. Woerdman, "Orbital angular momentum of light and the transformation of laguerre-gaussian laser modes," *Phys. Rev. A* **45**, pp. 8185–8189, Jun 1992.
5. M. E. J. Friese, J. Enger, H. Rubinsztein-Dunlop, and N. R. Heckenberg, "Optical angular-momentum transfer to trapped absorbing particles," *Phys. Rev. A* **54**, pp. 1593–1596, Aug 1996.
6. N. B. Simpson, K. Dholakia, L. Allen, and M. J. Padgett, "Mechanical equivalence of spin and orbital angular momentum of light: an optical spanner," *Opt. Lett.* **22**, pp. 52–54, Jan 1997.
7. G. Molina-Terriza, J. P. Torres, and L. Torner, "Management of the angular momentum of light: Preparation of photons in multidimensional vector states of angular momentum," *Phys. Rev. Lett.* **88**, p. 013601, Dec 2001.
8. A. Vaziri, G. Weihs, and A. Zeilinger, "Experimental two-photon, three-dimensional entanglement for quantum communication," *Phys. Rev. Lett.* **89**(24), p. 240401, 2002.
9. G. Molina-Terriza, J. P. Torres, and L. Torner, "Twisted photons," *Nature Physics* **3**(5), pp. 305–310, 2007.
10. A. van de Nes and P. Torok, "Rigorous analysis of spheres in gauss-laguerre beams," *Opt. Express* **15**, pp. 13360–13374, Oct 2007.
11. V. Garbin, G. Volpe, E. Ferrari, M. Versluis, D. Cojoc, and D. Petrov, "Mie scattering distinguishes the topological charge of an optical vortex: a homage to gustav mie," *New J. Phys.* **11**(1), p. 013046, 2009.
12. N. M. Mojarad and M. Agio, "Tailoring the excitation of localized surface plasmon-polariton resonances by focusing radially-polarized beams," *Opt. Express* **17**, pp. 117–122, Jan 2009.
13. D. Petrov, N. Rahuel, G. Molina-Terriza, and L. Torner, "Characterization of dielectric spheres by spiral imaging," *Opt. Lett.* **37**, pp. 869–871, Mar 2012.
14. A. S. Rury and R. Freeling, "Mie scattering of purely azimuthal laguerre-gauss beams: Angular-momentum-induced transparency," *Phys. Rev. A* **86**, p. 053830, Nov 2012.
15. M. R. Foreman, Y. Sivan, S. A. Maier, and P. Török, "Independence of plasmonic near-field enhancements to illumination beam profile," *Phys. Rev. B* **86**, p. 155441, Oct 2012.
16. X. Zambrana-Puyalto, X. Vidal, M. L. Juan, and G. Molina-Terriza, "Dual and anti-dual modes in dielectric spheres," *Opt. Express* **21**(15), pp. 17520–17530, 2013.
17. P. Woźniak, P. Banzer, and G. Leuchs, "Selective switching of individual multipole resonances in single dielectric nanoparticles," *Laser & Photonics Reviews* **9**(2), pp. 231–240, 2015.

18. X. Zambrana-Puyalto, X. Vidal, P. Woźniak, P. Banzer, and G. Molina-Terriza, "Tailoring multipolar mie scattering with helicity and angular momentum," *ACS Photonics* **5**(7), pp. 2936–2944, 2018.
19. J. Kindler, P. Banzer, S. Quabis, U. Peschel, and G. Leuchs, "Waveguide properties of single subwavelength holes demonstrated with radially and azimuthally polarized light," *Applied Physics B: Lasers and Optics* **89**(4), pp. 517–520, 2007.
20. G. Volpe, S. Cherukulappurath, R. J. Parramon, G. Molina-Terriza, and R. Quidant, "Controlling the optical near field of nanoantennas with spatial phase-shaped beams," *Nano Letters* **9**(10), pp. 3608–3611, 2009.
21. P. Banzer, J. Kindler, S. Quabis, U. Peschel, and G. Leuchs, "Extraordinary transmission through a single coaxial aperture in a thin metal film," *Opt. Express* **18**(10), pp. 10896–10904, 2010.
22. E. Hemo, B. Spektor, and J. Shamir, "Scattering of singular beams by subwavelength objects," *Appl. Opt.* **50**, pp. 33–42, Jan 2011.
23. J. Sancho-Parramon and S. Bosch, "Dark modes and fano resonances in plasmonic clusters excited by cylindrical vector beams," *ACS Nano* **6**(9), pp. 8415–8423, 2012.
24. X. Zambrana-Puyalto, X. Vidal, I. Fernandez-Corbaton, and G. Molina-Terriza, "Far-field measurements of vortex beams interacting with nanoholes," *Scientific Reports* **6**, p. 22185, 2016.
25. T. Bauer, S. Orlov, U. Peschel, P. Banzer, and G. Leuchs, "Nanointerferometric amplitude and phase reconstruction of tightly focused vector beams," *Nature Photonics* **8**(1), pp. 23–27, 2014.
26. S. Berg-Johansen, F. Töppel, B. Stiller, P. Banzer, M. Ornigotti, E. Giacobino, G. Leuchs, A. Aiello, and C. Marquardt, "Classically entangled optical beams for high-speed kinematic sensing," *Optica* **2**, pp. 864–868, Oct 2015.
27. M. Neugebauer, P. Woźniak, A. Bag, G. Leuchs, and P. Banzer, "Polarization-controlled directional scattering for nanoscopic position sensing," *Nat Commun.* **7**(1), pp. 1–6, 2016.
28. N. Tischler, J. Stark, X. Zambrana-Puyalto, I. Fernandez-Corbaton, X. Vidal, G. Molina-Terriza, and M. L. Juan, "All-optical self-referenced transverse position sensing with subnanometer precision," *ACS Photonics* **5**(9), pp. 3628–3633, 2018.
29. K. Toyoda, K. Miyamoto, N. Aoki, R. Morita, and T. Omatsu, "Using optical vortex to control the chirality of twisted metal nanostructures," *Nano letters* **12**(7), pp. 3645–3649, 2012.
30. X. Vidal, X. Zambrana-Puyalto, A. F. Barbara, I. Fernandez-Corbaton, and G. Molina-Terriza, "Chiral elements and dual systems: towards the design of an omnidirectional optical active media," in *Micro/Nano Materials, Devices, and Systems*, **8923**, p. 89233J, International Society for Optics and Photonics, 2013.
31. Y. Gorodetski, A. Drezet, C. Genet, and T. W. Ebbesen, "Generating far-field orbital angular momenta from near-field optical chirality," *Phys. Rev. Lett.* **110**, p. 203906, May 2013.
32. X. Zambrana-Puyalto, X. Vidal, and G. Molina-Terriza, "Angular momentum-induced circular dichroism in non-chiral nanostructures," *Nat. Commun.* **5**, p. 4922, 2014.
33. V. D'Ambrosio, G. Carvacho, F. Graffitti, C. Vitelli, B. Piccirillo, L. Marrucci, and F. Sciarrino, "Entangled vector vortex beams," *Phys. Rev. A* **94**, p. 030304, Sep 2016.
34. A. Büse, M. L. Juan, N. Tischler, V. D'Ambrosio, F. Sciarrino, L. Marrucci, and G. Molina-Terriza, "Symmetry protection of photonic entanglement in the interaction with a single nanoaperture," *Phys. Rev. Lett.* **121**, p. 173901, Oct 2018.
35. V. D'Ambrosio, G. Carvacho, I. Agresti, L. Marrucci, and F. Sciarrino, "Tunable two-photon quantum interference of structured light," *Phys. Rev. Lett.* **122**, p. 013601, Jan 2019.
36. X. Zambrana-Puyalto, X. Vidal, and G. Molina-Terriza, "Excitation of single multipolar modes with engineered cylindrically symmetric fields," *Opt. Express* **20**, pp. 24536–24544, Oct 2012.
37. X. Zambrana-Puyalto and G. Molina-Terriza, "The role of the angular momentum of light in mie scattering. excitation of dielectric spheres with laguerre-gaussian modes," *J. Quant. Spectrosc. Radiat. Transf.* **126**(0), pp. 50 – 55, 2013.
38. I. Fernandez-Corbaton, X. Zambrana-Puyalto, and G. Molina-Terriza, "Helicity and angular momentum: A symmetry-based framework for the study of light-matter interactions," *Phys. Rev. A* **86**, p. 042103, Oct 2012.

39. I. Fernandez-Corbaton, X. Zambrana-Puyalto, N. Tischler, X. Vidal, M. L. Juan, and G. Molina-Terriza, "Electromagnetic duality symmetry and helicity conservation for the macroscopic maxwell's equations," *Phys. Rev. Lett.* **111**, p. 060401, Aug 2013.
40. X. Zambrana-Puyalto, *Control and characterization of nano-structures with the symmetries of light.* PhD thesis, Macquarie University, 2014.
41. N. Tischler, I. Fernandez-Corbaton, X. Zambrana-Puyalto, A. Minovich, X. Vidal, M. L. Juan, and G. Molina-Terriza, "Experimental control of optical helicity in nanophotonics," *Light Sci Appl* **3**, p. e183, June 2014.
42. V. Grigoriev, S. Varault, G. Boudarham, B. Stout, J. Wenger, and N. Bonod, "Singular analysis of fano resonances in plasmonic nanostructures," *Phys. Rev. A* **88**, p. 063805, Dec 2013.
43. J. Mäkitalo, M. Kauranen, and S. Suuriniemi, "Modes and resonances of plasmonic scatterers," *Phys. Rev. B* **89**(16), p. 165429, 2014.
44. X. Zambrana-Puyalto and N. Bonod, "Purcell factor of spherical mie resonators," *Phys. Rev. B* **91**, p. 195422, May 2015.
45. N. Tischler, X. Zambrana-Puyalto, and G. Molina-Terriza, "The role of angular momentum in the construction of electromagnetic multipolar fields," *European journal of physics* **33**(5), p. 1099, 2012.
46. X. Zambrana-Puyalto *et al.*, "Probing the nano-scale with the symmetries of light," in *Journal and Proceedings of the Royal Society of New South Wales*, **147**(451/452), p. 55, Royal Society of New South Wales, 2014.
47. A. N. Oraevsky, "Whispering-gallery waves," *Quantum electronics* **32**(5), p. 377, 2002.
48. X. Zambrana-Puyalto and N. Bonod, "Tailoring the chirality of light emission with spherical si-based antennas," *Nanoscale* **8**, pp. 10441–10452, 2016.
49. X. Zambrana-Puyalto, I. Fernandez-Corbaton, M. L. Juan, X. Vidal, and G. Molina-Terriza, "Duality symmetry and kerker conditions," *Opt. Lett.* **38**, pp. 1857–1859, Jun 2013.
50. R. Neo, S. J. Tan, X. Zambrana-Puyalto, S. Leon-Saval, J. Bland-Hawthorn, and G. Molina-Terriza, "Correcting vortex splitting in higher order vortex beams," *Opt. Express* **22**, pp. 9920–9931, Apr 2014.